Available online at www.sciencedirect.com
ScienceDirect
Journal of Sound and Vibration 310 (2008) 1141–1166
JOURNAL OF SOUND AND VIBRATION
www.elsevier.com/locate/jsvi

Analysis of the energy transmission in spatial piping systems with heavy internal fluid loading

S.V. Sorokin[a,*], N. Olhoff[a], O.A. Ershova[b]

[a]Department of Mechanical Engineering, Aalborg University, Pontoppidanstraede 101, DK 9220 Aalborg, Denmark
[b]Department of Engineering Mechanics, State Marine Technical University, Lotsmanskaya Street #3, 190008 St. Petersburg, Russian Federation

Received 18 April 2007; received in revised form 14 August 2007; accepted 22 August 2007
Available online 24 October 2007

Abstract

The energy transmission in spatial elastic water-filled pipes is considered. A solution of the wave propagation problem in the framework of the general theory of elastic cylindrical shells with internal fluid loading is used as a reference. It is shown that energy transmission phenomena may be adequately described by means of the reduced theory in the frequency range of practical interest. The boundary integral equations method is specialised for this reduced theory and two generic problems of the energy transmission in piping systems are solved. The first one is concerned with analysis of the distribution of the transmitted energy between two branches in a pipeline with a single joint and between alternative transmission paths in each branch. Besides the frequency and the type of excitation, the influence of an angle between connected pipes is studied. The second problem is related to analysis of the energy transmission in a pipe with multiple regularly spaced junctions and attention is focused at formation of frequency band gaps due to periodicity of location of branches.

1. Introduction

Spatial piping systems are widely used in virtually all industrial and domestic applications, from gas- and oil-transporting pipelines to household heating and water supply systems. These systems are composed of elastic tubes, pumps and various appliances, for example, valves and radiators in heating systems. A by-product of the operational effect of pumps and valves is generation of vibro-acoustic energy, which may be transmitted in the pipeline over a long distance and emit undesirable noise, for example, from a radiator. The practical problem of reduction of noise emission from assembled pipelines with attached structures is closely linked with a necessity to study mechanisms of transportation of sound and vibration. Although duct acoustics and vibrations of tubular beams are well-established scientific subjects, an accurate and simple prediction of vibro-acoustic properties of spatial piping systems under heavy internal fluid loading is still not within reach. The physical explanation of such a state of the art is the complexity of wave propagation

*Corresponding author. Tel.: +45 96 35 93 32; fax: +45 98 15 16 75.
E-mail address: svs@ime.aau.dk (S.V. Sorokin).

0022-460X/$ - see front matter © 2007 Elsevier Ltd. All rights reserved.
doi:10.1016/j.jsv.2007.08.016

phenomena in such systems, in particular, the multiplicity of alternative transmission paths. This multiplicity manifests itself as a multiplicity of elements of a compound pipeline, which typically has several branches, possibly, with various geometry and material properties, as well as a multiplicity of co-existing propagating waves within each individual branch (dominantly axial waves, dominantly flexural waves, etc.). To be able to predict noise emission and to suggest efficient tools for its reduction in such a case, it is necessary to model an assembled structure and consider all coupling effects between its components.

Naturally, modelling is controlled by a frequency range and it is unrealistic to apply the same theoretical approach in any excitation conditions. The general discussion of alternative approaches, e.g., wave methods and statistical energy analysis methods, lies well beyond the scope of the present paper. It should be observed that the excitation of vibrations of and the energy transmission in pipelines in the frequency range from 60 to 100 Hz up to approximately 2–3 kHz is of particular concern in most of the industrial and domestic applications. For the standard pipes (see DIN2448), this is a low-frequency excitation, so that deterministic wave methods are perfectly suitable for the analysis. The task of modelling an assembled structure is accomplished in this paper by a systematic use of the methodology of boundary integral equations, elaborated in Refs. [1,2]. Then the problem of the energy transmission is formulated as a relatively low-order system of linear algebraic equations and its exact solution is readily available.

Although a straight pipe as such is an elastic cylindrical shell, it is not at all necessary to describe its behaviour always within the shell theory. The concept of modelling of long elastic pipes in the absence of fluid loading within the beam theory has been elaborated in many publications—see, for example, Refs. [3–5]. Respectively, the energy transmission is typically studied by means of the transfer matrix method, the spectral element method and their variations—see, for example, Refs. [6–8]. The methodology of boundary integral equations [1,2,9,10] offers a meaningful alternative to these methods, inasmuch it is equally applicable for the analysis of standing waves in systems of finite length and for the analysis of travelling waves in semi-infinite systems. Algebraic equations obtained by use of this method cannot be ill-conditioned because Green's functions used in their formulation satisfy the radiation and the decay conditions at infinity.

Spatial elastic piping systems can support propagation of waves of various types, which may be identified as dominantly longitudinal, torsional or flexural. In an infinitely long straight pipe modelled as a straight rod of tubular cross-section, these waves do not interact with each other. As soon as a compound pipe with branches is considered, the interaction between all these waves becomes essential. Apparently, this interaction is controlled by the angles between connected elements. The plane problem of interaction of flexural and longitudinal waves has been studied in numerous publications. For example, a sensitivity of the energy transmission in joints between beam plates has been analysed in Refs. [6,8]. Although the analysis reported in Ref. [8] is restricted to interacting flexural and longitudinal waves in two coupled plates, the results suggest that the energy distribution between alternative transmission paths may be highly sensitive to connection angle. It is natural to expect that similar phenomena could be observed in spatial elastic fluid-filled pipes. It is also relevant to consider various excitation situations, which are not always quite adequately described as an impinging wave, typically considered in literature. As soon as a piping system with multiple branches is considered, the periodicity effect (see, for example, Ref. [9]) should also be studied.

This paper addresses three aspects in analysis of the energy transmission in spatial compound elastic pipes, each of which presents aspects of novelty:

- formulation of the methodology of analysis of low-frequency wave propagation and energy transmission in fluid-filled pipes and assessment of its validity ranges,
- parametric studies of the energy transmission in generic junctions involving three pipe elements and
- parametric studies of the energy transmission in pipelines with several regularly spaced junctions.

The paper is structured in the following way. In Section 2, a simplified model of the energy transmission in elements of a compound piping system with and without internal heavy fluid loading is formulated and its validity is assessed. The methodology of analysis of wave propagation phenomena is outlined in Section 3. This section and its appendices present explicit formulation of Green's functions and boundary integral equations assembled with continuity/equilibrium conditions at the junctions between components of pipeline. As a simple illustration of the applicability of the methodology, the energy transmission through two typical

junctions is studied in Section 4 in relation to the power distribution between different types of travelling waves within each individual branch as a function of angles between pipes. Two typical assembled pipelines with several regularly spaced branches are considered in Section 5. The analysis of the energy distribution between their elements in various excitation conditions is extended to the study of formation of the stop-band phenomenon. Results of the analysis are summarised in Section 6.

2. On modelling of spatial piping systems composed of thin elastic cylindrical shells with and without heavy internal fluid loading

A general theory of elastic cylindrical shells (with and without heavy internal fluid loading) is valid to describe wave propagation phenomena in piping systems under arbitrary excitation conditions and it is 'sufficiently' simple to analyse the energy transmission in straight pipes. However, its application becomes rather involved when compound spatial pipelines are considered (for example, as shown in Fig. 1). In this case, wave interaction phenomena at branching points imply coupling between waves with different circumferential wavenumbers, which is generated due to the obvious fact that the whole compound structure ceases to be axi-symmetric. The energy transmission analysis is complicated at sufficiently high frequencies, when elements of a fluid-filled pipeline support a moderate number of propagating waves, and it becomes very challenging in a high-frequency range, when the wavelengths become comparable with the diameters of the pipes.

As discussed in the Introduction, the excitation of industrial and domestic fluid-filled pipelines occurs at relatively low frequencies. In terms of the energy transmission analysis, the low-frequency range may be defined by the condition that the excitation frequency lies below its cut-on values for modes with $m>1$ (m is a circumferential wavenumber). In this case, the general theory of elastic fluid-filled cylindrical shells predicts the existence of only four propagating waves (their cut-on frequencies equals zero). One of those is a wave of dominantly flexural deformation at $m=1$ (the bending mode). Three other ones are axi-symmetric ($m=0$): a pure torsion wave (it does not experience any influence of fluid inside a pipe as long as viscosity effects can be neglected), a dominantly structural longitudinal wave and a dominantly acoustical 'duct' wave (the two 'breathing' modes). A balance of the energy transmission between alternative (structural and acoustical) paths in the latter two modes has been studied in Ref. [10].

In this frequency range, it is reasonable to assume that complicated local effects of interaction between multiple evanescent waves existing in branches of a spatial pipeline do not alter the energy transmission to a far field, which occurs only at propagating modes. Besides, lengths of propagating waves are large in comparison with diameters of connected pipes. Then it is possible to reduce the problem of analysis of wave propagation and energy transmission in a spatial piping system to its one-dimensional formulation. Such a formulation, in effect, stems from an asymptotic analysis of equations of low-frequency wave propagation in cylindrical shells, which results in simplified equations for flexural, torsion, axial and acoustical waves.

To conclude discussion of reduction of the problem in hand to its one-dimensional formulation, an important qualification should be made: it is anticipated that the energy exchanges between co-existing propagating waves in a near field may be modelled with only flexural evanescent waves involved. In other words, at low frequencies the dominant energy exchanges occur in the boundary layer of flexural deformation

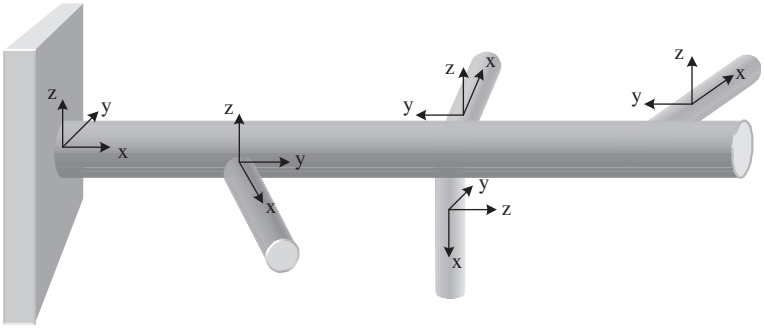

Fig. 1. A compound pipe.

of a pipe. The assessment of validity of this intuitively reasonable assumption constitutes the current research area of the authors.

The applicability of conventional beam theory for analysis of propagation of flexural waves in elastic cylindrical shells has been studied in a number of references, for example, Refs. [11–13]. However, a possibility to extend this theory to capture propagation of flexural waves in the case of heavy internal fluid loading has gained less attention in literature (see Ref. [14]). To the best of authors' knowledge, the same holds true regarding formulation of elementary theories of propagation of axial and torsion waves in elastic cylindrical shells filled with a compressible fluid.

Consider a cylindrical shell filled with an acoustic medium (see Fig. 2). Material properties of a shell, which has the thickness h and the radius of its mid-surface R, are specified by the density ρ, Young's modulus E and Poisson ratio ν. The density of the fluid is introduced as ρ_{fl} and the sound speed is c_{fl}.

The formulation of the problem of wave propagation is very well known. For consistency, it is given in Appendix A. Dispersion curves, which are obtained from this problem formulation, are used as a reference solution to control applicability of simplified models reported in the subsequent subsection.

2.1. Simplified models

Probably the most 'natural' type of motion of a long tube is its vibration in the 'beam-type' mode, i.e., when the number of circumferential waves is $m = 1$. Although the general theory (see Appendix A) is perfectly valid in this case, a considerable simplification of equations reported in Appendix A may be introduced to speed up computations needed to obtain characteristics of wave propagation. Specifically, it is reasonable to assume, that no distortion of the cross-sectional shape occurs in this case and displacements are linked with each other as

$$v_1(x) = -w_1(x), \tag{1a}$$

$$u_1(x) = -R\,\frac{\mathrm{d}w_1(x)}{\mathrm{d}x}. \tag{1b}$$

Then the following single differential equation of beam-like motion of a shell with fluid loading is obtained

$$\frac{Eh}{1-\nu^2}\left(R^2+\frac{h^2}{12}\right)w_1'''' + \rho_0 hR^2\omega^2 w_1'' - 2\rho_0 hR^2\omega^2 w_1 + \mathrm{i}\rho_{\mathrm{fl}}\omega\varphi_1 = 0. \tag{2}$$

The velocity potential φ_1 is still governed by the differential equation (A.1d) and the boundary condition (A.1e).

The shear force resultant and the bending moment resultant (as the terminology of conventional beam theory is adopted) acting in the whole cross-section of a pipe are formulated as

$$Q = \frac{\pi ERh}{1-\nu^2}\left(R^2+\frac{h^2}{12}\right)\frac{\mathrm{d}^3 w_1}{\mathrm{d}x^3}, \tag{3a}$$

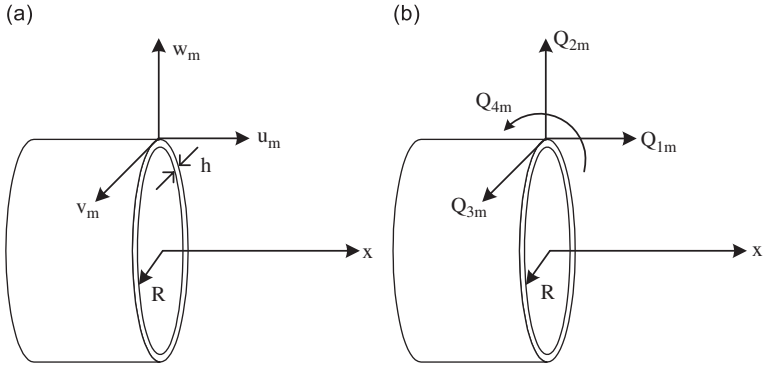

Fig. 2. A cylindrical shell: (a) displacements and (b) force and moment resultants.

$$M = \frac{\pi E R h}{1-\nu^2}\left(R^2 + \frac{h^2}{12}\right)\frac{\mathrm{d}^2 w_1}{\mathrm{d}x^2}. \tag{3b}$$

It is remarkable to note that this simple 'beam' theory is equally applicable to study wave motion in a cylindrical shell filled by a compressible or an incompressible fluid since the assumptions (1a), (1b) do not concern the behaviour of the fluid inside the tube.

It is possible to simplify Eq. (2) by taking the limit $c_{\mathrm{fl}} \to \infty$ (or, in other words, to ignore fluid's compressibility). Then a model of flexural wave propagation in a fluid-filled beam with a tubular cross-section is given by an elementary differential equation

$$\frac{Eh}{1-\nu^2}\left(R^2 + \frac{h^2}{12}\right)w_1'''' + \rho_0 h R^2 \omega^2 w_1'' - \rho_0 h R^2 \omega^2 \left(2 + \frac{\rho_{\mathrm{fl}}}{\rho_0}\frac{R}{h}\right)w_1 = 0. \tag{4}$$

As follows from this equation, a fluid simply contributes to the inertial properties of a tube so that particles of the fluid exactly follow transverse motions of the tube at each cross-section, i.e., fluid inside a pipe behaves as a purely inertial inclusion, which has no stiffness. Inasmuch a solution of the exact equation (A.7) is available it does not present any difficulty to assess the range of validity of Eq. (4).

It is also a simple exercise to show that the Eq. (4) asymptotically ($\omega \to 0$, $h/R \to 0$) merges the elementary equation of the flexural beam-type propagating wave in the conventional Bernoulli–Euler theory for a pipe filled in with purely inertial medium

$$EI_y w_1'''' - (\rho_0 A + \rho_{\mathrm{fl}} A_{\mathrm{fl}})\omega^2 w_1 = 0, \tag{5}$$

$$I_y = \frac{\pi d_{\mathrm{out}}^4}{64}\left(1 - \frac{d_{\mathrm{in}}^4}{d_{\mathrm{out}}^4}\right), \quad A = \frac{\pi d_{\mathrm{out}}^2}{4}\left(1 - \frac{d_{\mathrm{in}}^2}{d_{\mathrm{out}}^2}\right), \quad A_{\mathrm{fl}} = \frac{\pi d_{\mathrm{in}}^2}{4}, \quad d_{\mathrm{in}} = 2R - h, \quad d_{\mathrm{out}} = 2R + h.$$

The formulation of bending moment and shear force in cross-section of a pipe is standard: $M_y = EI_y w_1''$, $Q_z = EI_y w_1'''$. Eq. (5) is very well known and may be found, for example, in Ref. [5]. It should be observed, however, that this equation yields a mismatch with the shell theory due to the difference in assumptions concerning strains and stresses in cross-sections. Specifically, Bernoulli–Euler theory is formulated for an uni-axial stain–stress relation, $\varepsilon_x = (\sigma_x/E)$. It implies that the circumferential stress vanishes, $\sigma_\theta = 0$. In opposite, kinematic hypotheses (1) postulate absence of any distortion of circular cross-section of a pipe, i.e., $\varepsilon_\theta = 0$. Then one obtains the standard formula for plane strain state: $\varepsilon_x = ((1-\nu^2)\sigma_x)/E$. This issue has been thoroughly discussed, for example, in Ref. [15]. As is shown in the subsection, which follows this one, the dispersion curve predicted by the theory (4) is in excellent agreement with their counterpart predicted by the exact theory.

In the case of axi-symmetric modes ($m = 0$), Eq. (A.1) are factorised into two sets. The first one describes torsion wave

$$-\frac{1-\nu}{2}\frac{\mathrm{d}^2 v_0}{\mathrm{d}x^2} - \frac{h^2}{12}\frac{2(1-\nu)}{R^2}\frac{\mathrm{d}^2 v_0}{\mathrm{d}x^2} - \frac{\rho\omega^2(1-\nu^2)}{E}v_0 = 0. \tag{6}$$

This equation has an elementary counterpart in the theory of straight rods

$$GI_{\mathrm{p}}\frac{\mathrm{d}^2\phi}{\mathrm{d}x^2} + \rho\omega^2 I_{\mathrm{p}}\phi = 0. \tag{7}$$

Here $\phi(x) = (v_0(x)/R)$ is a torsion angle, $G = E/(2(1+\nu))$, $I_p = ((\pi d_{\mathrm{out}}^4)/32)(1 - (d_{\mathrm{in}}^4/d_{\mathrm{out}}^4))$. Similarly to the case of a flexural wave, Eq. (6) asymptotically merges Eq. (7) as $(h/R) \to 0$.

The second set of equations, which follows from (A.1) at $m = 0$, describes the coupled axial, flexural and acoustic waves in a fluid-filled shell:

$$-\frac{\mathrm{d}^2 u_0}{\mathrm{d}x^2} - \frac{\nu}{R}\frac{\mathrm{d}w_0}{\mathrm{d}x} - \frac{\rho\omega^2(1-\nu^2)}{E}u_0 = 0, \tag{8a}$$

$$\frac{\nu}{R}\frac{\mathrm{d}u_0}{\mathrm{d}x}+\frac{1}{R^2}\,w_0+\frac{h^2}{12}\frac{\mathrm{d}^4w_0}{\mathrm{d}x^4}-\frac{\rho\omega^2(1-\nu^2)}{E}\,w_0-\frac{\mathrm{i}\omega\rho_{\mathrm{fl}}(1-\nu^2)R}{Eh}\,\varphi_0=0, \tag{8b}$$

$$\frac{\partial^2\varphi_0}{\partial r^2}+\frac{1}{r}\frac{\partial\varphi_0}{\partial r}+\frac{\partial^2\varphi_0}{\partial x^2}+\frac{\omega^2}{c_{\mathrm{fl}}^2}\,\varphi_0=0, \tag{8c}$$

$$\left.\frac{\partial\varphi_0}{\partial r}\right|_{r=R}=-\mathrm{i}\omega w_0. \tag{8d}$$

Detailed asymptotic analysis of this system of equations lies beyond the scope of the present paper, but the zero-order approximation to its solution corresponds to the total decoupling between axial, acoustical and flexural waves.

Specifically, the flexural axi-symmetric wave is described as

$$\frac{1}{R^2}\,w_0+\frac{h^2}{12}\frac{\mathrm{d}^4w_0}{\mathrm{d}x^4}-\frac{\rho\omega^2(1-\nu^2)}{E}w_0=0. \tag{9}$$

As is clearly seen, it cuts on at high frequencies (above a 'ring frequency' $(\rho\omega_{\mathrm{ring}}^2(1-\nu^2)R^2)/E=1$), so that it is not involved in the energy transmission at low frequencies.

The longitudinal wave may approximately be described by a reduced equation

$$-\frac{\mathrm{d}^2u_0}{\mathrm{d}x^2}-\frac{\rho\omega^2(1-\nu^2)}{E}\,u_0=0. \tag{10}$$

This equation is identical to the equation of propagation of a longitudinal wave in a rod of an annular cross-section under assumption that circumferential deformation is absent, $\varepsilon_\theta\equiv(w_0/R)=0$:

$$\frac{E}{1-\nu^2}A\,\frac{\mathrm{d}^2u_0}{\mathrm{d}x^2}+\rho\omega^2Au_0=0,\quad A=\frac{\pi d_{\mathrm{out}}^2}{4}\left(1-\frac{d_{\mathrm{in}}^2}{d_{\mathrm{out}}^2}\right). \tag{11}$$

The dominantly acoustic plane 'duct' wave, $\varphi_0=\varphi_0(x)$, may be described by another reduced equation

$$\frac{\mathrm{d}^2\varphi_0}{\mathrm{d}x^2}+\frac{\omega^2}{c_{\mathrm{fl}}^2}\,\varphi_0=0. \tag{12}$$

In this case, the boundary condition (8d) has become redundant, since $\varphi_0=\varphi_0(x)$ and $w_0=0$. Naturally, at this level of approximation a terminology introduced to describe longitudinal and acoustic waves as 'breathing' becomes incorrect: pressure pulsations and longitudinal displacements do not produce any radial 'breathing' displacements.

To summarise this sub-section, in a low frequency range it is possible to use four simplified models, which virtually emerge from the theory of rods and duct acoustics, rather than general theory of elastic cylindrical shells under internal heavy fluid loading. Naturally, the case of absence of internal fluid loading is captured by setting $\rho_{\mathrm{fl}}=0$ in Eq. (8b). Then an acoustic wave vanishes from the analysis.

2.2. Validity ranges of the simplified models

Eqs. (4), (6), (10), (12) model propagation of flexural, torsional, longitudinal and acoustic waves in an elastic fluid-filled cylindrical shell. Inasmuch they are derived under several 'questionable' assumptions, it is necessary to straightforwardly estimate their validity by comparison of dispersion curves they predict with dispersion curves that follow from the exact problem formulation (A.1). However, applicability of this elementary modelling of the energy transmission phenomena in spatial piping systems is controlled not only by accuracy in description of travelling waves captured in this modelling. It is equally essential to check that all 'high-order' waves, which cannot be described by the above-mentioned elementary equations, are of the evanescent type.

Dispersion equations follow from Eqs. (4), (6), (10), (12) as their solutions are sought in the form (A.2). Specifically, the dispersion equation for flexural wave acquires the following form ($\Omega=\omega R/c$,

$c^2 = E/(\rho(1-v^2))$, $\tilde{\rho} = \rho/\rho_{\mathrm{fl}}$, $\tilde{\gamma} = c/c_{\mathrm{fl}}$, $k = k_{\mathrm{dim}}R$):

$$\left(1+\frac{h^2}{12R^2}\right)k^4 + \Omega^2 k^2 - 2\Omega^2 - \tilde{\rho}\Omega^2\frac{R}{h} = 0. \tag{13}$$

The dispersion equation for a torsion wave is

$$\left(1+\frac{h^2}{3R^2}\right)k^2 + \frac{2}{1-v}\,\Omega^2 = 0. \tag{14}$$

The dispersion equation for an axial wave is

$$k^2 + \Omega^2 = 0. \tag{15}$$

The dispersion equation for an acoustical wave is

$$k^2 + \tilde{\gamma}^2\Omega^2 = 0. \tag{16}$$

For definiteness, consider two standard pipes from DN2448. The first one has the outer diameter $D_{\mathrm{out}} = 48.3$ mm and wall thickness $h = 2.6$ mm. In the paper, it is referred to as a small pipe. The second pipe has $D_{\mathrm{out}} = 76.1$ mm and $h = 2.9$ mm. In both cases, the material is steel, $E = 2\times10^5$ MPa, $\rho = 7800\,\mathrm{kg/m^3}$, $v = 0.3$. Pipes are filled in with water, $\rho_{\mathrm{fl}} = 1000\,\mathrm{kg/m^3}$, $c_{\mathrm{fl}} = 1400\,\mathrm{m/s}$. In the paper, it is referred to as a large pipe.

In Figs. 3a, b dispersion curves after Eqs. (13)–(16) are plotted as solid lines and dispersion curves after exact solution ((A.5), (A.6)) are presented by dots for the first and the second pipe, respectively. Curve 1 presents a flexural wave, curve 2 presents an acoustical wave, curve 3 presents a torsion wave and curve 4 presents an axial wave. The elementary theory cannot predict the propagating wave at $m = 2$ (curve 5).

As is seen from these graphs, elementary Eqs. (13)–(16) are valid to describe propagation of waves in fluid-filled pipes in a broad frequency range. For the first pipe, it is $0<f<2300$ Hz. For the second pipe, it is $0<f<950$ Hz. The limitation of their applicability is determined by the requirement that an excitation frequency should be below the cut-on frequency of the shell mode $m = 2$. Above this frequency, the wavenumbers of propagating waves are still predicted accurately by these models, but the energy transmission cannot be adequately described because the propagating shell mode $m = 2$ is not captured.

It is also helpful to compare the minimum wave lengths with the diameter of a pipe. In the former case, the shortest wavelength (in a flexural wave) at the threshold frequency of around 2.3 kHz is $L_{\mathrm{wave}} \approx 20R$. For the second pipe, it is $L_{\mathrm{wave}} \approx 18R$ at the threshold frequency of 950 Hz. Thus, in both cases, zones, where pipes are connected (see Fig. 1) are compact in terms of wavelengths and the one-dimensional formulation of the wave propagation problem is justified.

The conclusion in the case of a pipeline without heavy fluid loading is obvious: the modelling of wave propagation in a system of arbitrarily connected straight pipes in the framework of elementary theory introduced by Eqs. (4), (6) and (10) is perfectly valid. In other words, the energy is transmitted by the flexural, torsional and longitudinal waves in a rod of annular cross-section, which adequately models an elastic cylindrical shell as long as the excitation frequency does not exceed the cut-on frequency of the mode $m = 2$. It should be just noted that in a compound pipe with several branches it is necessary to introduce two flexural waves in orthogonal planes, say, vertical and horizontal in Fig. 1. The methodology of boundary integral equations may conveniently be applied to yield an exact solution of the problem of the energy distribution between different branches of a piping system and between alternative propagating waves in each branch.

In the case of a fluid-filled compound pipe, the situation is more difficult. The torsion wave (6) is not influenced by the presence of a fluid and the dominantly flexural wave is governed by a modified Eq. (4), which takes into account for added mass correction. However, the dominantly longitudinal wave and the dominantly acoustic 'duct' wave are coupled via the radial displacement in a shell as is defined by the exact set of Eq. (8) and, therefore called 'breathing'. As has been shown in Ref. [10] the energy distribution between these two waves is very sensitive to excitation conditions and the dominantly acoustic 'duct' wave is generated primarily by axi-symmetric monopole-type sources in a fluid. Such a source is realistic, it is provided, for example, as an operational effect of a pump (a pressure pulsation at the blade passing frequency). Another possibility to efficiently excite this wave is the action of a radial load uniformly distributed over the circumference of a pipe.

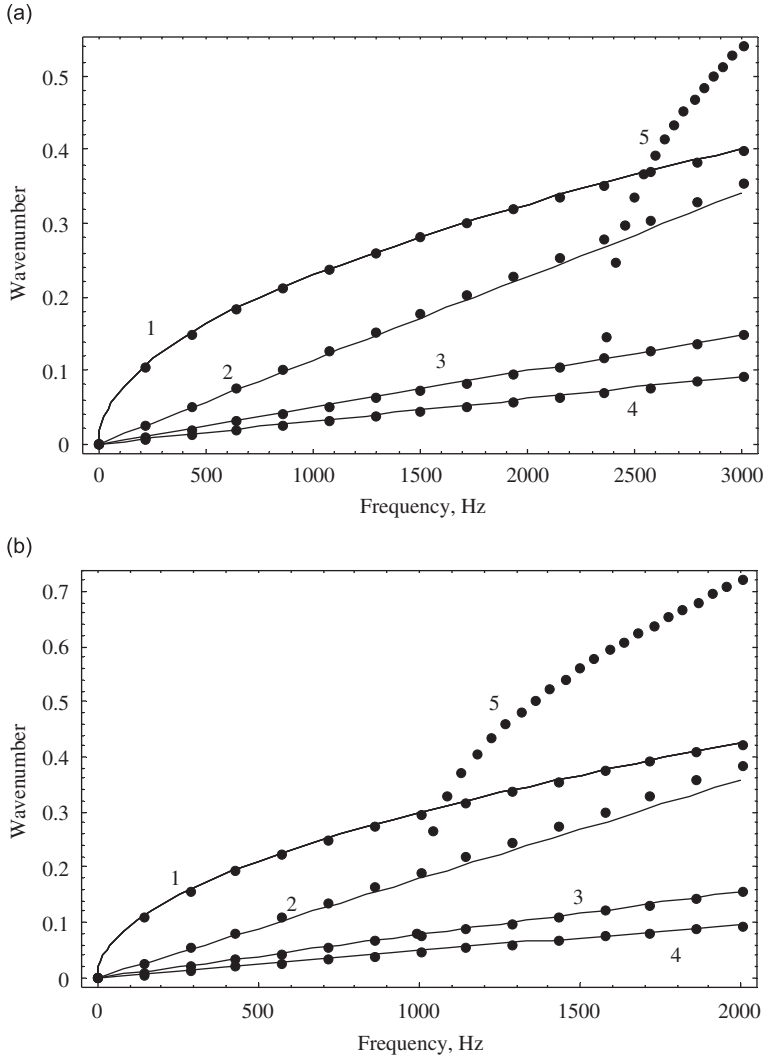

Fig. 3. Dispersion curves for (a) small pipe and (b) large pipe.

Unlike the previously considered case, such a mechanical excitation is much less typical in industrial and domestic applications. The structural longitudinal axi-symmetric wave can be directly excited by action of an axial load uniformly distributed over the circumference of a pipe. This type of excitation is not typical, but, as is shown in Section 4, a longitudinal wave may easily be excited at the joints between components of a spatial piping system.

As is also discussed in Ref. [10], the energy exchanges between the dominantly structural and dominantly acoustical waves in the low frequency excitation regime are very weak. It means that once the dominantly acoustical 'duct' wave is excited, it does not interact with the dominantly structural longitudinal wave and vice versa. Therefore, it is reasonable to adopt a simplified approach to analysis of the energy transmission in elastic pipelines with heavy internal fluid loading in the considered frequency range. Specifically, the energy transmission by dominantly structural waves may be considered as uncoupled from the energy transmission by the dominantly acoustic duct wave. This simplification is supported by the fact that, in the frequency range of interest, each of these waves is rather accurately described by uncoupled asymptotically reduced Eqs. (10) and (12). It facilitates use of the methodology of boundary integral equations to analyse interaction between structural (i.e., flexural, torsional and longitudinal) waves in a pipeline with multiple branches. The same

methodology can be used for analysis of propagation of dominantly duct acoustic waves in pipelines. However, this analysis may conveniently be performed by other techniques, see, for example, Refs. [16,17]. It should be emphasised that the proposed decomposition is justified only in the low-frequency range. At higher frequencies, the coupling between acoustic and structural waves becomes more pronounced and also the shell modes begin to propagate.

3. The methodology of analysis of wave propagation in compound spatial piping systems

For definiteness, the system of coordinates in each element is shown in Fig. 1 so that the following equations in non-dimensional form describe time harmonic deformation of a pipe (displacements and the axial coordinate are scaled by the radius of the pipe, and index n now stands for the number of an element):

- flexural deformation in a XOZ (vertical) plane

$$\left(1+\frac{h^2}{12R^2}\right)\frac{\mathrm{d}^4 w_n}{\mathrm{d}x^4}+\Omega^2\frac{\mathrm{d}^2 w_n}{\mathrm{d}x^2}-\Omega^2\left(2+\frac{\rho_{\mathrm{fl}}}{\rho_0}\frac{R}{h}\right)w_n=\frac{q_z(1-\nu^2)R}{Eh}, \tag{17a}$$

- flexural deformation in a XOY (horizontal) plane

$$\left(1+\frac{h^2}{12R^2}\right)\frac{\mathrm{d}^4 v_n}{\mathrm{d}x^4}+\Omega^2\frac{\mathrm{d}^2 v_n}{\mathrm{d}x^2}-\Omega^2\left(2+\frac{\rho_{\mathrm{fl}}}{\rho_0}\frac{R}{h}\right)v_n=\frac{q_y(1-\nu^2)R}{Eh}, \tag{17b}$$

- torsion deformation

$$\left(1+\frac{h^2}{3R^2}\right)\frac{\mathrm{d}^2\phi_n}{\mathrm{d}x^2}+\frac{2}{1-\nu}\Omega^2\phi_n=-\frac{m_\theta(1-\nu^2)}{Eh}, \tag{17c}$$

- axial deformation

$$\frac{\mathrm{d}^2 u_n}{\mathrm{d}x^2}+\Omega^2 u_n=-\frac{q_x(1-\nu^2)R}{Eh}. \tag{17d}$$

Right-hand sides of these equations contain intensities of forces distributed at the surface of a pipe. Specifically, q_x, q_y, q_z are intensities of external pressure components acting in directions of local coordinates shown in Fig. 1, and m_θ is the intensity of torque.

Wave propagation in the piping system presented in Fig. 1 may conveniently be described by boundary integral equations. Green's functions in explicit form are presented in Appendix B. For each element of a piping system extended from $x=a$ to $x=b$, Somigliana identities are presented in Appendix B. As is seen from Eqs. (A.2)–(A.4), 12 non-dimensional unknowns at each edge of a tubular element are introduced:

- three displacements, $u_n(x)$, $v_n(x)$, $w_n(x)$,
- three angles, $\phi_n(x)$, $v_n'(x)$, $w_n'(x)$,
- three components of a scaled force resultant,

$$N_{xn}(x)\equiv\frac{1-\nu^2}{\pi ERh}N_{xn}^{\dim}(x)=u_n'(x),$$
$$Q_{yn}(x)\equiv\frac{1-\nu^2}{\pi ERh}Q_{yn}^{\dim}(x)=\left(1+\frac{h^2}{12R^2}\right)v_n'''(x),$$
$$Q_{zn}(x)\equiv\frac{1-\nu^2}{\pi ERh}Q_{zn}^{\dim}(x)=\left(1+\frac{h^2}{12R^2}\right)w_n'''(x),$$

- three components of a scaled moment resultant,

$$M_{xn}(x) \equiv \frac{1-\nu^2}{\pi ERh}\, M_{xn}^{\dim}(x) = \frac{1-\nu}{2}\left(1+\frac{h^2}{3R^2}\right)\phi_n'(x),$$
$$M_{yn}(x) \equiv \frac{1-\nu^2}{\pi ERh}\, M_{yn}^{\dim}(x) = \left(1+\frac{h^2}{12R^2}\right)w_n''(x),$$
$$M_{zn}(x) \equiv \frac{1-\nu^2}{\pi ERh}\, M_{zn}^{\dim}(x) = \left(1+\frac{h^2}{12R^2}\right)v_n''(x).$$

The identities (A.2) and (7)–(12) yield six boundary equations at the edges as the observation point tends to them from inside the element, $\xi = a+\varepsilon$, $\xi = b-\varepsilon$, $\varepsilon \to 0$. If a semi-infinite element is considered ($b \to \infty$), then Eqs. (A.2) and (7)–(12) do not contain contributions at $x = b$.

The system of governing algebraic equations is accomplished with boundary conditions for the 'end' elements, see, for example, element 1 in Fig. 1 and with the junctions conditions at the branching points. These conditions consist of six continuity conditions for generalised displacements and six equilibrium conditions. They are presented in Appendix C for two typical junctions considered in Section 4.

As soon as this system is solved, the identities (A.2) and (7)–(12) may be used for calculations of displacements, slopes, forces and moments at any cross-section of the piping system. The energy transmission in a pipe includes the following components:

- the energy in axial wave

$$\tilde{E}_{\mathrm{a}}(x) = -\frac{1}{2}\,\mathrm{Re}[N_x(x)\dot{u}^*(x)], \tag{18a}$$

- the energy in torsional wave

$$\tilde{E}_t(x) = -\frac{1}{2}\,\mathrm{Re}[M_x(x)\,\dot{\phi}^*(x)], \tag{18b}$$

- the energy in flexural wave in the plane XOY

$$\tilde{E}_{\mathrm{fl},z}(x) = -\frac{1}{2}\,\mathrm{Re}[Q_y(x)\dot{w}^*(x) - M_z(x)\dot{w}'^*(x)], \tag{18c}$$

- the energy in flexural wave in the plane XOZ

$$\tilde{E}_{\mathrm{fl},y}(x) = -\frac{1}{2}\,\mathrm{Re}[Q_z(x)\dot{v}^*(x) - M_y(x)\dot{v}'^*(x)]. \tag{18d}$$

In these formulas, complex conjugates of translational and rotational velocities (second terms in each product) are designated by dots and stars. Naturally, if the energy dissipation is neglected, then each component of the conveyed energy is independent upon axial coordinate within the element.

As already discussed, it is assumed that, once generated, the dominantly acoustical plane 'duct' wave does not interact with these dominantly structural waves. As long as coupled Eq. (8) are replaced by their reduced counterparts (10) and (12), the acoustic energy transmission may be considered in an uncoupled formulation of the problem. The distribution of this energy component between the same acoustical plane 'duct' waves in branches can easily be modelled by appropriate boundary equations, but this task lied beyond the scope of

the paper. The re-distribution of the energy between four structural components in branches is modelled by the equations presented in Appendix A and C.

The codes implementing this methodology has been checked in several test cases via comparison of eigenfrequencies of empty and fluid-filled homogeneous and compound cylindrical shells with the analytical results, results obtained by use of this methodology in the framework of general thin shell theory [1,4] and results of finite element analysis in ANSYS [18].

This methodology should not be mixed up with a transfer matrices methodology in various formulations (as, for example, the spectral element method). The distinctive feature of the boundary integral equations method in analysis of wave propagation in quasi-one-dimensional waveguides is that its formulation employs only outgoing and decaying waves. In ultimately simple cases of an acoustic plane wave, or an axial wave, or a torsion wave, elements of Green's matrix as well as transfer matrix present only contributions of propagating waves, inasmuch evanescent waves are not supported in these waveguides. However, in the case of flexural deformation of a tubular beam and in the case, when the shell theory is used, it is necessary to take into account also for non-propagating waves. Straightforward formulation of transfer matrix involves simultaneous presence of exponentially growing and decaying waves. It may bring to numerical instabilities, especially when a shell is thin and long. These instabilities indicate that the boundary layers at the edges of a shell (or tubular beam) weakly interact with each other. The Green's matrices and boundary integral equations methodology is advantageous in these cases as it guarantees stability of computations.

4. Analysis of the energy transmission in typical branching junctions

The methodology presented in the previous Section may be used for analysis of wave propagation in various piping systems with multiple arbitrary located junctions. As a simple example, consider the energy transmission in two typical structures, each of which has only one 'bifurcation' into branches.

4.1. Planar structure

Probably, the simplest case of a pipe with two branches is shown in Fig. 4a. The 'main' straight pipe (elements 1 and 3) is connected with a branch 2. This figure represents the case, when elements 1, 3 are made of 'large' pipes, whereas element 2 is made of 'small' pipe. The left edge of the first element is clamped (see Fig. 4a), its length is denoted as L_0. Elements 2 and 3 are semi-infinite. Consider firstly the case, when all three elements are made of small steel pipes (they have the same outer diameter $D_{\text{out}} = 48.3\,\text{mm}$ and wall thickness $h = 2.6\,\text{mm}$. For definiteness, consider a pipe filled with water and let the span be $L_0 = 2\,\text{m}$.

The excitation is produced by point unit force acting along one of the coordinate axes or by a unit torque. Location of excitation point is denoted as x_e. The system of linear algebraic equations to be solved in the general case contains 48 unknowns. However, this system can always be factorised to two sub-systems, because two types of coupled waves do not interact with each other. The first type of waves is a coupled torsion and bending in the vertical plane that is referred to as out-of-plane motion. It is excited by a vertical force as seen in Fig. 4b or, alternatively, by a torque. The in-plane motion is produced by bending in the horizontal plane and axial deformation. It is excited by a horizontal force as seen in Fig. 4c or, alternatively, by an axial force.

The unit force is applied in the horizontal plane as shown in Fig. 4c. In Fig. 5a, b, the energy input into the pipe versus excitation frequency is presented by full line for $\alpha = \pi/2$, $x_e = 0.2$ (Fig. 5a) and $\alpha = \pi/2$, $x_e = 0.8$ (Fig. 5b). As a reference, dotted curve is plotted for a homogeneous pipe (a pipe without branch 2). The energy input in arbitrary excitation conditions is formulated as a sum of contributions (18) calculated at the loaded cross-section. Naturally, as long as the energy dissipation is neglected, this sum may be calculated at any cross-section of the first segment between the loading point and the junction, see Fig. 4.

As is seen from comparison of these graphs, the locations of minima and maxima of the continuous curves are virtually insensitive to the position of the excitation point, whereas the shapes of the dotted curves are very different. It has a simple explanation: the shapes of dotted curves for a homogeneous pipe are controlled by the 'mirror effect', which is governed by the ratio between the length of the propagating flexural wave and the distance from the excitation point to the clamped edge, which is different in these two cases. The shapes of

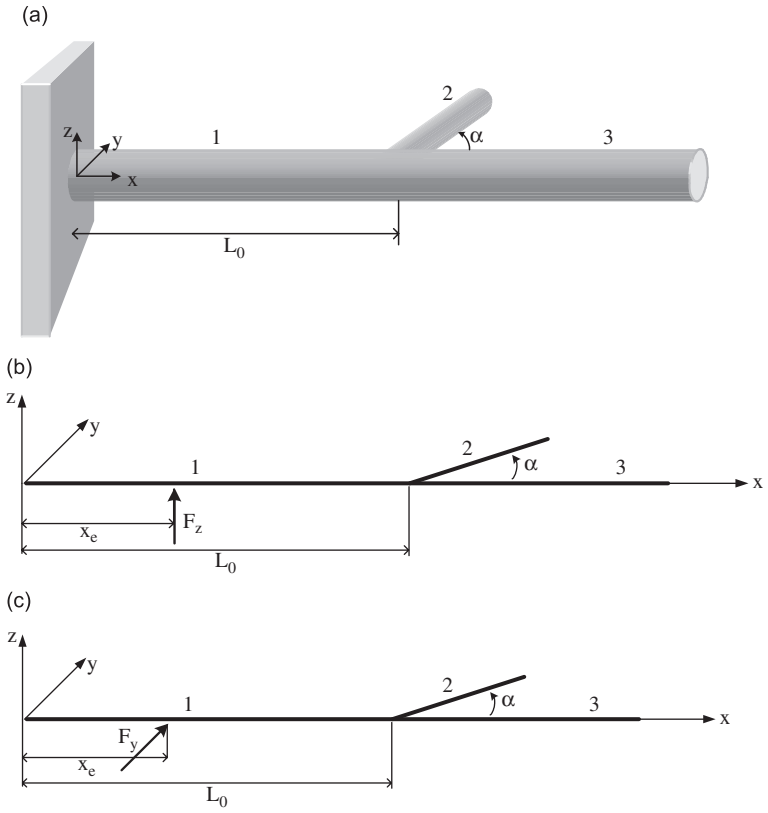

Fig. 4. A planar structure (a) and its out-of-plane (b) and in-plane (c) excitation.

continuous curves are controlled by the distance between the clamped edge and the junction point, which is kept constant. The peaks in these curves characterise resonant frequencies of the element 1 being considered as clamped at the left edge. This 'isolated' element would have its right edge being supported by a spring and a dashpot.

The influence of angle α on energy distribution between alternative transmission paths is illustrated in Fig. 6a, b plotted for $f = 330$ and 512 Hz (the maxima of the energy injected to an inhomogeneous pipe, see Fig. 5a) in the case of an in-plane excitation. The total input is shown by curve 1. The energy is distributed between the flexural wave in straight element 3 (curve 2), the axial wave in element 3 (curve 3), the flexural wave in side branch element 2 (curve 4), the axial wave in element 2 (curve 5). All numerical data is scaled by the energy input produced by the same force into a homogeneous pipe, so that, for example, curve 2 presents $I_{\mathrm{fl}}^{(3)} = E_{\mathrm{fl},z}^{(3)}/E_{\mathrm{hom}}^{(3)}$ (naturally, E_{hom} is independent of the angle). As is seen, the energy is distributed rather unevenly between alternative transmission paths and its distribution is frequency-dependent.

In the case of $\alpha = 0$, the input energy is evenly distributed between two identical branches. It is interesting to observe that the energy distribution is virtually insensitive to variations in the magnitude of the angle α up to $\alpha \approx 0.2$. To some extent, the same holds true for small deviations of the angle from its other limit, $\alpha = \pi/2$. In this layout of a pipe, the dominant energy component is the energy transmitted by an axial wave in the side branch (curve 5). Maxima of sensitivities of the energy distribution components to the angle are located in different points, as is seen from Fig. 6. In both cases, one can find a threshold angle separating the regime of the energy transmission dominated by the flexural wave in the straight branch from the regime dominated by the axial wave in the side branch.

There are also some differences between these two cases. The most important one is the difference in dependence of the total power input upon the angle. In the latter case, this quantity attains a maximum at $\alpha \approx 1.1$. In the former case, it increases monotonously. The energy conveyed by flexural waves (curves 2, 4) is

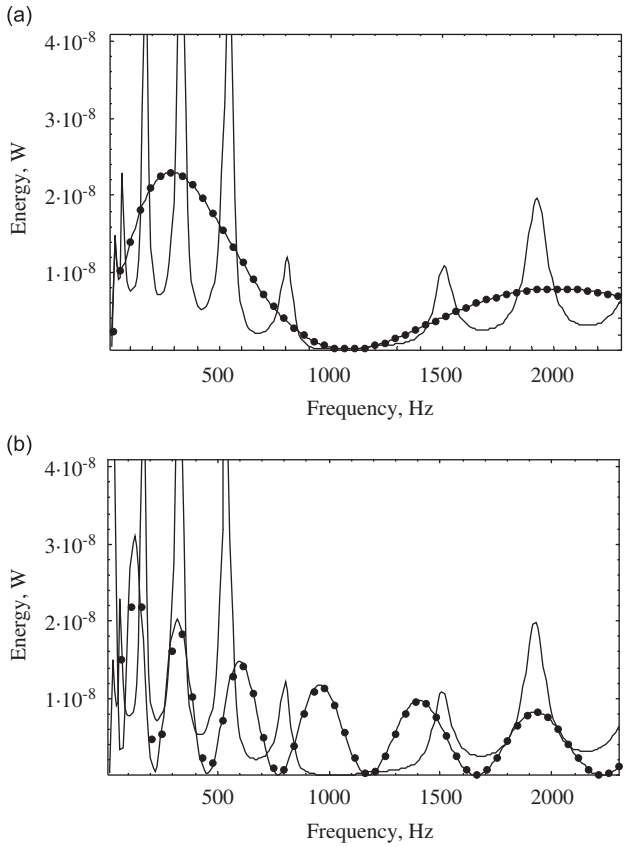

Fig. 5. The injected energy versus excitation frequency, in-plane (horizontal) unit force: (a) $x_e = 0.2$ and (b) $x_e = 0.8$. Full curve represents inhomogeneous pipe and dotted curve homogeneous pipe.

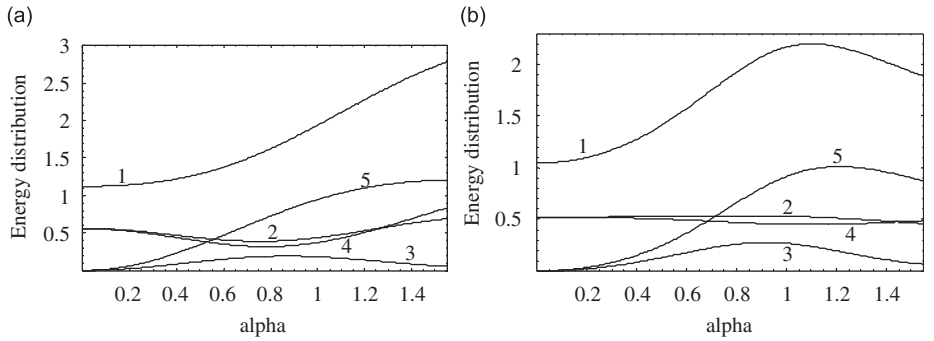

Fig. 6. The influence of angle α on energy distributions, (a) $f = 330\,\text{Hz}$, $x_e = 0.2$ and (b) $f = 512\,\text{Hz}$, $x_e = 0.2$.

virtually insensitive to the magnitude of α at $f = 512\,\text{Hz}$, whereas it has a minimum attained simultaneously by these curves at $\alpha \approx 0.8$ when $f = 330\,\text{Hz}$. The amount of energy transmitted in the element 3 by the axial wave (curve 3) attains a maximum approximately at the same angle. These results suggest that the energy transmission in such a typical junction is fairly sensitive to the excitation frequency.

In Figs. 6a, b, ratios of energy components relative to the energy input in a homogeneous pipe are presented for a fixed location of an excitation point, $x_e = 0.2$. It is relevant to explore the dependence of energy components on this parameter. As follows from graphs presented in Fig. 5, the energy input into a

homogeneous pipe is very sensitive to the location of the excitation point. However, the distribution of the energy between components (but not their magnitudes) is independent upon the location of the excitation point. This is illustrated in Fig. 7 for the pipe with $\alpha = \pi/2$ at excitation frequency $f = 330\,\mathrm{Hz}$. For convenience, curves are labelled in the same way as in the previous graph, but curve 1 is not drawn (it should present unit value).

The dependence of the scaled energy flow components on the excitation frequency is shown in Fig. 8. The driving force is applied at $x_e = 0.8$. The angle between branches 2 and 3 is $\alpha = \pi/2$. As is seen from this figure, the dominant path of the energy transmission in the frequency range $500\,\mathrm{Hz} < f < 2300\,\mathrm{Hz}$ is in a longitudinal wave in the side branch element 2 (curve 5). At virtually any frequency within this range, the portion of energy conveyed by the flexural wave in each element is approximately the same and it is a half of the energy conveyed by a longitudinal wave in element 2.

Now consider excitation of out-of-plane vibrations by a vertical force (see Fig. 4b). Graphs in Fig. 9a,b are counterparts of those in Fig. 5a,b. An obvious conclusion that follows from comparison of these graphs is that out-of-plane excitation, which couples flexural and torsion waves, is substantially less influenced by the presence of branching. The injected energy attains maxima at the same frequencies as in the case of in-plane excitation, but their magnitudes are much smaller.

To explain this result, it is expedient to analyse the energy distributions among different components as a function of the angle α. In Fig. 10 the energy conveyed by the flexural wave in element 2 is shown as curve 4, by the torsion wave in element 2 as curve 5, by the flexural wave in element 3 as curve 2, by the torsion wave in

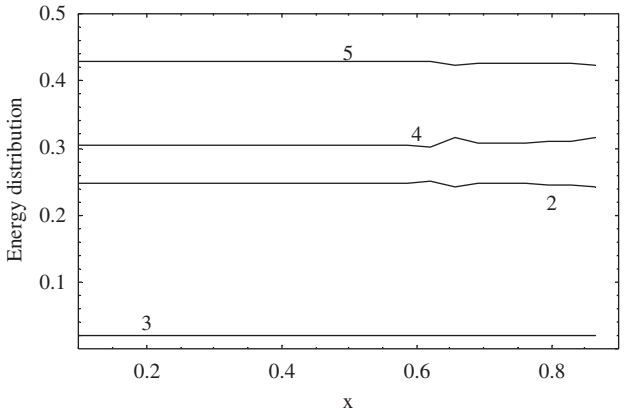

Fig. 7. The influence of x_e on energy distributions, $\alpha = \pi/2$, $f = 330\,\mathrm{Hz}$.

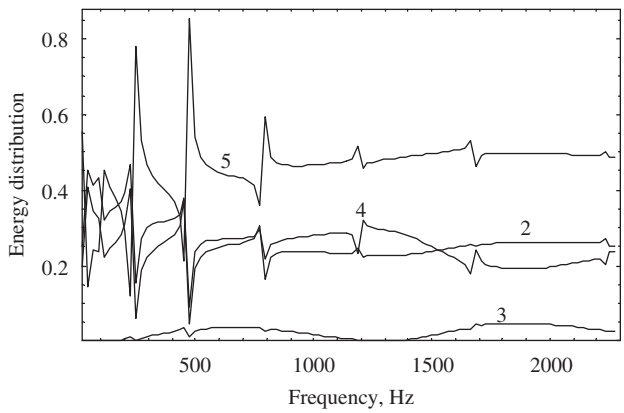

Fig. 8. The influence of excitation frequency on energy distributions, $\alpha = \pi/2$, $x_e = 0.8$.

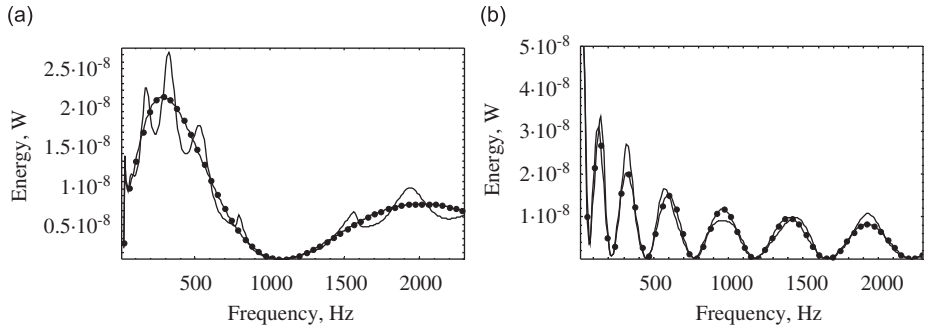

Fig. 9. The injected energy versus excitation frequency, out-of-plane (vertical) unit force: (a) $x_e = 0.2$ and (b) $x_e = 0.8$. Full curve represents inhomogeneous pipe and dotted curve homogeneous pipe.

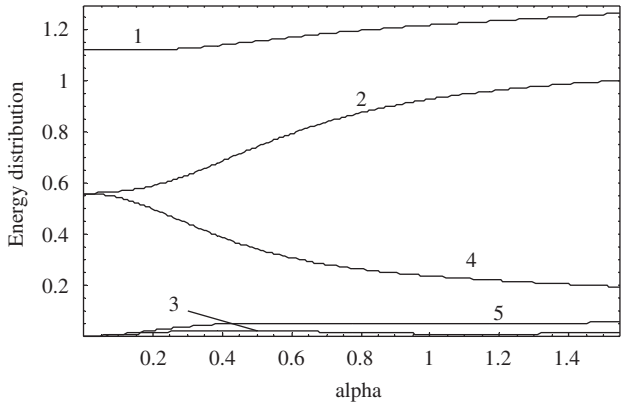

Fig. 10. The influence of angle α on energy distributions, $f = 330\,\text{Hz}$, $x_e = 0.2$.

element 3 as curve 3. The total input is shown as curve 1. All numerical data is scaled by the energy input produced by the same force into a homogeneous pipe, so that, for example, curve 2 presents $\Gamma_{\text{fl}} = E_{\text{fl},y,2}/E_{\text{hom}}$ (E_{hom} is, of course, independent of the angle).

As is seen, the torsional wave carries a relatively small amount of energy in the whole range $0 < \alpha < (\pi/2)$. The dominant transmission path appears to be a flexural wave in the element 2. Therefore, the torsional wave in element 2 does not serve as an efficient 'energy sink' in the case of out-of-plane excitation.

Alternative excitations by an axial force and by a torque are reciprocal to those already considered here. Specifically, the out-of-plane torsion excitation is featured similarly to in-plane excitation by a horizontal force, and the in-plane axial excitation is similar to out-of-plane excitation by a vertical force.

4.2. Spatial structure

In the 'planar branching' considered in the previous sub-section, two uncoupled sets of waves exist. The simplest structural layout, which couples in-plane and out-of-plane excitation cases, is shown in Fig. 11. The planar structure with $\alpha = \pi/2$ is recovered in this model, when $\beta = 0$. The main purpose of the analysis of the spatial structure is to study how significant the coupling between in-plane and out-of-plane waves is. Therefore, all three elements are considered to be the same, i.e. small steel pipes. Naturally in this case for $\beta = \pi/2$, there is no difference between vertical and horizontal excitation. The energy injected into the pipe in this layout as a function of the excitation frequency is shown in Fig. 12a, b by a thin continuous curve. For convenience, the dotted curve presents the energy input into a homogeneous pipe (they are the same as in Fig. 5a, b).

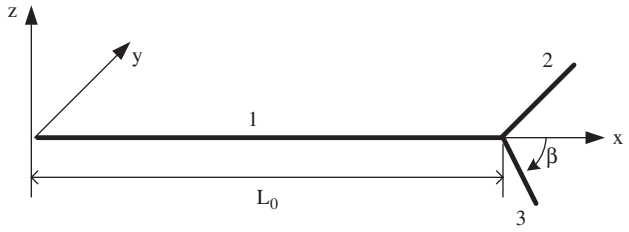

Fig. 11. A spatial structure. Branch 2 is parallel to the y-axis, and branch 3 is lying in the xz-plane.

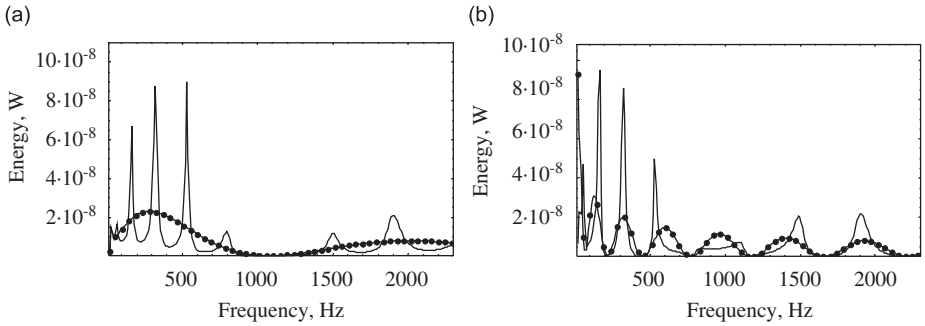

Fig. 12. The injected energy versus excitation frequency, unit force at (a) $x_e = 0.2$ and (b) $x_e = 0.8$. Full curve represents inhomogeneous pipe and dotted curve homogeneous pipe.

As is seen from comparison of graphs in Figs. 5 and 12, the resonant trapped mode effect is amplified in the case of a spatial structure. However, the locations of the maxima in Fig. 12 are not strongly shifted as compared with Fig. 5, because the 'effective stiffness' of elements 2, 3 is not too much different from the effective stiffness of element 3 in the planar structure.

The distribution of energy is illustrated in Fig. 13 for the horizontal excitation and in Fig. 14 for the vertical excitation as sketched in Fig. 4c. Notations are the same in all Figures. The total energy input is shown by curve 1. The energy is distributed between the flexural wave in element 2 in the horizontal plane XOY (curve 2), the flexural wave in element 2 in the vertical plane XOZ (curve 3), the axial wave in element 2 (curve 4), the torsion wave in element 2 (curve 5), the flexural wave in element 3 in the inclined plane (curve 6), the flexural wave in element 3 in the vertical plane XOZ (curve 7), the axial wave in element 3 (curve 8). Since many components are weakly involved in the energy transmission, all Figures are plotted not from zero in the vertical axis. Therefore only those exceeding a certain threshold value, which can be seen in the coordinate frame in each figure, are shown. As before, all numerical data is scaled by the energy input produced by the same force into a homogeneous straight pipe.

The energy distribution at $\beta = 0$ is the same as the energy distribution at $\alpha = \pi/2$ in Figs. 6a, b. Curves 2, 4 and 6 in Figs. 13a, b are continuations of, correspondingly, curves 5, 4 and 2 in Fig. 6a,b. Graphs in Fig. 13a are plotted starting from 0.1. At both frequencies, variation in the angle β does not alter the dominant transmission paths. The most of energy is conveyed by the flexural and the longitudinal wave in the side branch 2. In other words, the in-plane excitation is not strongly affected by the presence of the out-of-plane branches. This conclusion may be drawn from comparison of in-plane and out-of-plane excitation of a planar structure.

The energy distribution is rather sensitive to both the excitation frequency and to the angle β, and it is dangerous to come up with certain general design recommendations. For example at $f = 330$ Hz, the total energy input decreases with the growth in β, whereas at $f = 512$ Hz, the total energy input attains maximum approximately at $\beta \approx 1.25$. This maximum, however, does not coincide with maxima of the energy in the longitudinal waves in element 2 (curve 4) and element 3 (curve 8).

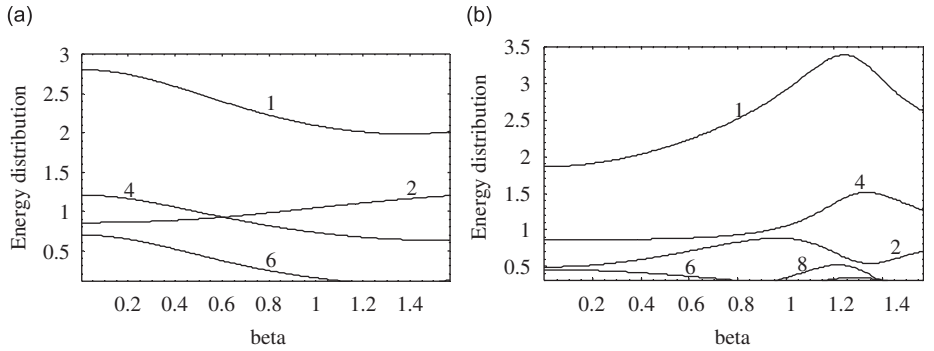

Fig. 13. The influence of angle β on energy distributions, excitation by a horizontal force (a) $f = 330\,\text{Hz}$, $x_e = 0.2$ and (b) $f = 512\,\text{Hz}$, $x_e = 0.2$.

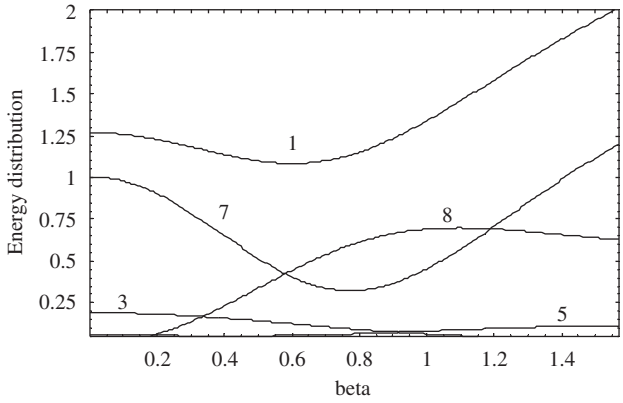

Fig. 14. The influence of angle β on energy distributions, $f = 330\,\text{Hz}$, $x_e = 0.2$, excitation by a vertical force.

Graphs in Fig. 14 are plotted for excitation by a vertical force applied at the same point $x_e = 0.2$ as in the case of excitation by a horizontal force. The energy distribution at $\beta = \pi/2$ is identical to that shown in Fig. 13a. In another limit case, $\beta = 0$, the energy distribution is the same as shown in Fig. 10 for $\alpha = \pi/2$.

At $\beta = 0$, the energy is conveyed dominantly by the flexural wave in a vertical plane. This energy distribution changes only at relatively large angle, $\beta \approx 0.2$. The energy transmission by the axial wave in the element 3 becomes dominant in the range $0.6 < \beta < 1.2$. Starting from this range of frequencies, the total energy input also increases. As the angle approaches its limit value $\beta = \pi/2$ at this excitation frequency, the dominant transmission path (the flexural wave in the element 3) is restored. However, at other frequencies, for example at 512 Hz, the most of energy is conveyed in an axial wave in element 3, see Fig. 13b.

As follows from results reported in this Section, the energy distribution between different transmission paths is very sensitive to excitation parameters. From a practical point of view this means that an optimisation of the energy transfer in a compound pipe may be efficient only if the excitation conditions are well defined.

5. Analysis of the energy transmission in two piping systems with several branches

Consider now piping systems with several branches. For simplicity (as well as to explore the periodicity effect), assume that a pipe is composed by 'self-repeating' elements, which are introduced in the previous section.

5.1. Planar structure

The planar structure is composed of repeated elements shown in Fig. 4. They are connected as shown in Fig. 15 and the distance between branches L_1 may be different from the length of the loaded span L_0. The left edge of the first span is fully clamped as shown in Fig. 4a. This model introduces many parameters (diameters of elements, distances between them, number of branches, type of excitation, etc.) and detailed analysis of their influence on the energy transmission lies beyond the scope of this paper.

As an illustrative example, consider the influence on the energy transmission of a number of identical branches with the same distance between each other. They are made of steel and they have the outer diameter $D_{\text{out}} = 48.3\,\text{mm}$ and wall thickness $h = 2.6\,\text{mm}$. The first span has the length $L_0 = 2\,\text{m}$, the distance between branches is $L_1 = 0.8\,\text{m}$. Each side branch is attached at the same angle $\alpha = \pi/2$. The pipeline is filled with water.

Consider in-plane excitation of this structure by a horizontal force (see Fig. 4c) applied at $x_e = 0.2$. The energy input as a function of the excitation frequency is shown in Fig. 16 by the upper thin full curve. The total energy input into the semi-infinite homogeneous pipe without branches is shown by the dotted curve. This curve is the same as in Fig. 5a. Another thin full curve located much below the two others presents the energy transported in an infinitely long element directed along the axis x, see Fig. 15. This energy may be called the energy output, because it is conveyed to the remote part of a piping system. The substantial reduction in the energy output in the whole frequency range is attributed to the presence of three additional branches.

In Fig. 17a, curves 1, 2, 3 present the 'suppression coefficient' $-10\lg(E_{\text{out}}/E_{\text{hom}})$ for three layouts of the structure. In the first layout, the pipe consists of three elements as is shown in Fig. 4, $\alpha = \pi/2$. In the second layout, the pipeline has two side branches. The third layout is shown in Fig. 15.

As is seen from Fig. 17a, the reduction in the energy transmission is substantially amplified by adding elements of periodicity. To characterise this effect in one more way, the 'suppression coefficient' in the form $-10\lg(E_{\text{out}}/E_{\text{in}})$ is presented in Fig. 17b. This figure highlights generation of the frequency band gap around $1100\,\text{Hz} < f < 1600\,\text{Hz}$, where the suppression coefficient grows. This phenomenon in fluid-filled shells has been reported in Ref. [1].

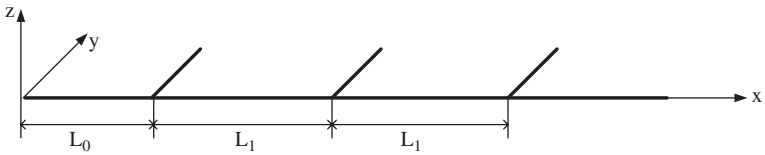

Fig. 15. A planar structure with three branches.

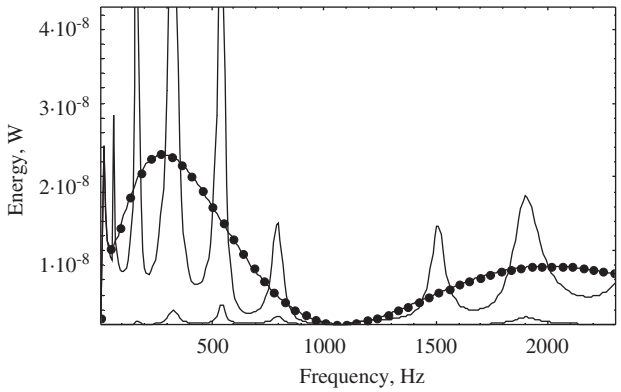

Fig. 16. The energy input and output in a planar piping system.

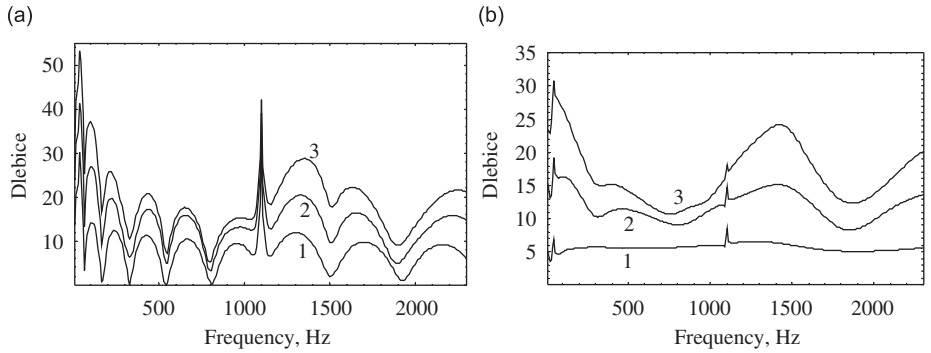

Fig. 17. Attenuation of the energy transmission in the case of in-plane excitation (a) the 'suppression coefficient' $-10\lg(E_{out}/E_{hom})$ (b) the 'suppression coefficient' in the form $-10\lg(E_{out}/E_{in})$.

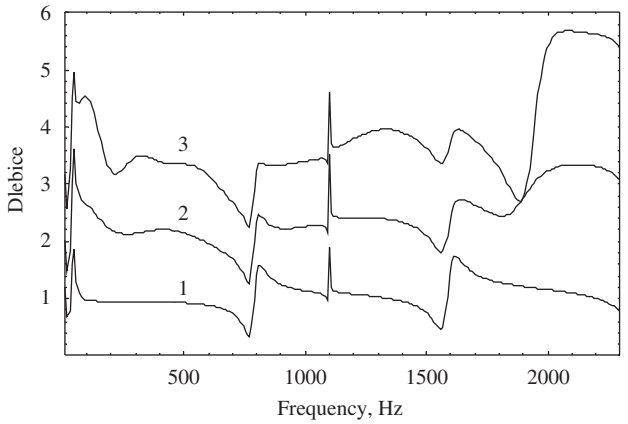

Fig. 18. Attenuation of the energy transmission in the case of out-of-plane excitation.

In the case of out-of-plane excitation by a unit vertical force applied at the same point $x_e = 0.2$, the efficiency of the energy transmission suppression is much lower. This result matches the analysis reported in Section 5. In Fig. 18, the 'suppression coefficient' in the form $-10\lg(E_{out}/E_{in})$ is shown. As is seen, it increases only by 1–2 Db with addition of extra side branches, whereas each additional side branch gives around 10 Db in suppression of the energy transmission in the case of in-plane excitation.

In practice, a pipeline with multiple branches is likely to be composed of pipes of different diameters. The main straight pipe normally has a diameter larger that the diameter of side pipes. As a relevant example, consider the main large pipe with small branches. Their dimensions are given in Section 3. As shown, the approximate theory for analysis of the energy transmission in a large pipe is valid up to $f \approx 900$ Hz (the cut-on frequency of the 'ovalling mode' $m = 2$). The coefficients $-10\lg(E_{out}/E_{hom})$ and $-10\lg(E_{out}/E_{in})$ versus excitation frequency are shown in Fig. 19a, b for the in-plane excitation.

5.2. Spatial structure

Finally, consider for consistency the energy transmission in the periodic piping system composed of self-repeated elements shown in Fig. 12 for $\beta = \pi/2$. The 'last element', however, has one more infinite branch extended along x-axis, see Fig. 20.

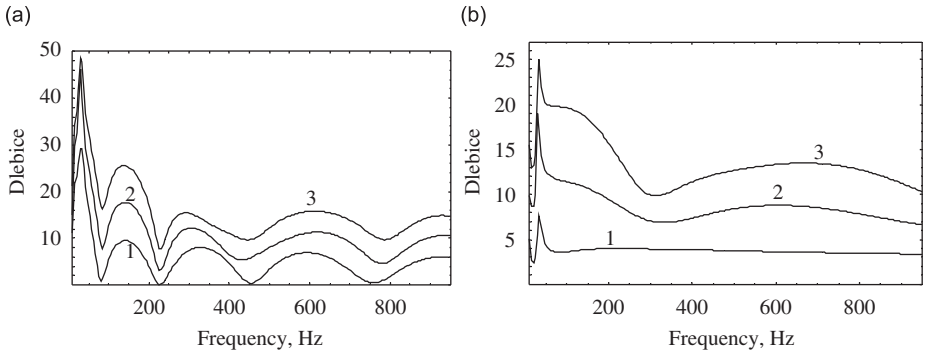

Fig. 19. Attenuation of the energy transmission in the case of in-plane excitation (a) the 'suppression coefficient' $-10\lg(E_{out}/E_{hom})$ (b) the 'suppression coefficient' in the form $-10\lg(E_{out}/E_{in})$.

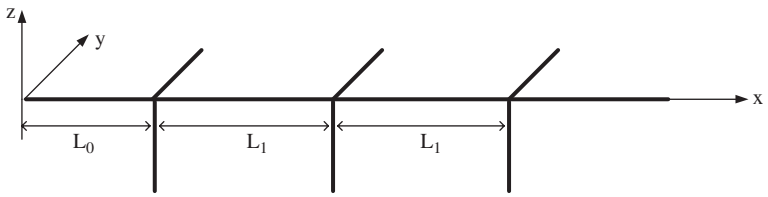

Fig. 20. A spatial structure composed of three periodicity cells.

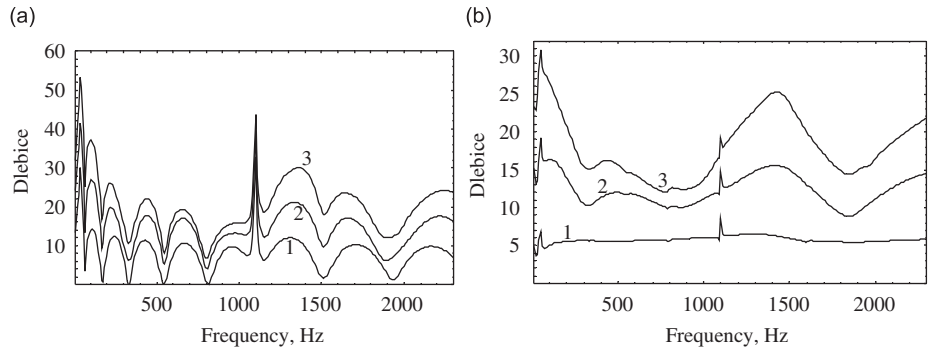

Fig. 21. Attenuation of the energy transmission (a) the 'suppression coefficient' $-10\lg(E_{out}/E_{hom})$ (b) the 'suppression coefficient' in the form $-10\lg(E_{out}/E_{in})$.

Identical branches are located within the same distance between each other. They are made of steel and have the outer diameter $D_{out} = 48.3$ mm and wall thickness $h = 2.6$ mm. The first span has the length $L_0 = 2$ m, and the distance between branches is $L_1 = 0.8$ m. Each set of side branches is attached at the same angles $\alpha = \pi/2$ and $\beta = \pi/2$. The pipeline is filled with water. The graphs in Figs. 21a, b should be compared with their counterparts shown in Figs. 18a,b. As expected, double branching does not produce a significant amplification of the trapped mode effect in comparison with in-plane excitation of a planar structure. This is due to weakness of the periodicity effect observed in the case of out-of plane excitation of a planar structure. Apparently, an advantage of the double branching is its robustness to possible variation in direction of the force.

The stop band effect clearly demonstrated in this Section is linked to the trapped mode effect, well known in the theory of waveguides with inclusions (the 'simplest' trapped mode has been described in Ref. [19]). Localisation (an exponential decay in the amplitude) of vibrations in the vicinity of an isolated discontinuity (e.g., inclusion) in an unbounded waveguide observed at a distinct frequency (the trapped mode effect) is amplified and expanded to continuous stop bands due to multiplicity of inclusions. In the limit case of an infinite set of inclusions, this stop band effect is described by classic Floquet theory. As reported in Refs. [1,9], significant trapping stop band effect is achievable when a few periodicity cells are involved.

In the context of analysis of vibrations of fluid-filled pipes, this effect should not be regarded as unconditionally advantageous. Although it reduces the amount of the energy transmitted to the remote part of a piping system, it inevitably results in high levels of vibrations of the pipe element where the force is applied. Therefore, the issues of high sound pressure levels in a compartment, where a pump is mounted and possible fatigue of the pipe should be taken into account.

Although the methodology presented in this paper is perfectly valid to analyse modes of forced vibrations of spatial piping systems, and, in fact, in each case reported in this paper the mode of forced vibrations is readily available, such an investigation is deliberately left out of the scope of the present contribution concerned with the energy transmission issues.

6. Conclusions

The results reported in this paper may be summarised as follows:

- The methodology of boundary integral equations is specialised for analysis of the time-harmonic behaviour of compound fluid-filled spatial piping systems and its validity range is assessed.
- The wave interaction and the energy transmission phenomena in the case of planar piping systems are strongly dependent upon the type of excitation. In the case of in-plane excitation by a transverse force, side branches serve as an efficient energy sink, associated with generation of a longitudinal wave in it. In the case of out-of-plane excitation by a transverse force, the same side branch does not consume a large amount of energy.
- In the modelling of realistic assembled pipelines, it is important to specify excitation conditions more precisely than an impinging wave of a given type, because the presence of a reflecting edge of a segment exposed to the excitation produces a substantial effect on the energy transmission phenomena.
- The existence of 'high-sensitive' ranges of connection angles is typical for structural layouts considered. The location of these high-sensitive angle ranges is frequency-dependent.
- The alternative energy transmission paths are 'highly competitive' and the dominance of a single one relative to others is strongly dependent upon geometry parameters (angles of connection) and excitation conditions (excitation frequency and type of forcing).
- The periodicity effect is clearly observed in pipelines with a number of equally spaced identical side branches.

Appendix A. General formulaton of the problem of wave propagation in an elastic cylindrical shell with heavy internal fluid loading

The governing equations, which describe propagation of free waves in a cylindrical shell filled with a compressible fluid, in the dimensional form are

$$-\frac{\mathrm{d}^2 u_m}{\mathrm{d}x^2}+\frac{1-\nu}{2}\frac{m^2}{R^2}u_m-\frac{1+\nu}{2}\frac{m}{R}\frac{\mathrm{d}v_m}{\mathrm{d}x}-\frac{\nu}{R}\frac{\mathrm{d}w_m}{\mathrm{d}x}-\frac{\rho\omega^2(1-\nu^2)}{E}u_m=0, \tag{A.1a}$$

$$\begin{aligned}&\frac{1+\nu}{2}\frac{m}{R}\frac{\mathrm{d}u_m}{\mathrm{d}x}-\frac{1-\nu}{2}\frac{\mathrm{d}^2 v_m}{\mathrm{d}x^2}+\frac{m^2}{R^2}v_m-\frac{h^2}{12}\frac{2(1-\nu)}{R^2}\frac{\mathrm{d}^2 v_m}{\mathrm{d}x^2}+\frac{h^2}{12}\frac{m^2}{R^4}v_m+\frac{m}{R^2}w_m\\&+\frac{h^2}{12}\frac{m^3}{R^4}w_m-\frac{h^2}{12}\frac{(2-\nu)m}{R^2}\frac{\mathrm{d}^2 w_m}{\mathrm{d}x^2}-\frac{\rho\omega^2(1-\nu^2)}{E}v_m=0,\end{aligned} \tag{A.1b}$$

$$\frac{v}{R}\frac{\mathrm{d}u_m}{\mathrm{d}x}+\frac{m}{R^2}v_m+\frac{h^2}{12}\frac{m^3}{R^4}v_m-\frac{h^2}{12}\frac{(2-v)m}{R^2}\frac{\mathrm{d}^2v_m}{\mathrm{d}x^2}+\frac{1}{R^2}w_m+\frac{h^2}{12}\frac{\mathrm{d}^4w_m}{\mathrm{d}x^4}-\frac{h^2}{12}\frac{2m^2}{R^2}\frac{\mathrm{d}^2w_m}{\mathrm{d}x^2}+\frac{h^2}{12}\frac{\mathrm{m}^4}{R^4}w_m-\frac{\rho\omega^2(1-v^2)}{E}w_m-\frac{\mathrm{i}\omega\rho_{\mathrm{fl}}(1-v^2)R}{Eh}\varphi_m=0, \tag{A.1c}$$

$$\frac{\partial^2\varphi_m}{\partial r^2}+\frac{1}{r}\frac{\partial\varphi_m}{\partial r}-\frac{m^2}{r^2}\varphi_m+\frac{\partial^2\varphi_m}{\partial x^2}+\frac{\omega^2}{c_{\mathrm{fl}}^2}\varphi_m=0, \tag{A.1d}$$

$$\left.\frac{\partial\varphi_m}{\partial r}\right|_{r=R}=-\mathrm{i}\omega w_m. \tag{A.1e}$$

In these equations, (u_m, v_m, w_m) are components of the vector of displacements of a shell in the axial, circumferential and radial directions, respectively (see Fig. 2), and φ_m is a velocity potential. The positive direction of a radial displacement coincides with the positive direction of a radial coordinate. The index m in these equations defines the number of circumferential waves in the considered mode

$$\begin{aligned}u(x,\theta,t)&=u_m(x)\cos(m\theta)\exp(-\mathrm{i}\omega t),\\ v(x,\theta,t)&=v_m(x)\sin(m\theta)\exp(-\mathrm{i}\omega t),\\ w(x,\theta,t)&=w_m(x)\cos(m\theta)\exp(-\mathrm{i}\omega t),\\ \varphi(x,\theta,r,t)&=\varphi_m(x,r)\cos(m\theta)\exp(-\mathrm{i}\omega t).\end{aligned}$$

Due to the axial symmetry of a shell, there is no coupling between waves with different circumferential wavenumbers. A solution to the set of homogeneous differential Eq. (A.1) is sought as

$$\begin{aligned}u_m(x)&=A_m\exp(k_{\mathrm{dim}}x),\\ v_m(x)&=B_m\exp(k_{\mathrm{dim}}x),\\ w_m(x)&=C_m\exp(k_{\mathrm{dim}}x),\\ \varphi_m(x,r)&=\hat{\varphi}_m(r)\exp(k_{\mathrm{dim}}x).\end{aligned} \tag{A.2}$$

where k_{dim} is a dimensional wavenumber and propagating waves correspond to its purely imaginary values

The function $\hat{\varphi}_m(r)$ is determined from the following reduced problem:

$$\frac{\mathrm{d}^2\hat{\varphi}_m}{\mathrm{d}r^2}+\frac{1}{r}\frac{\mathrm{d}\hat{\varphi}_m}{\mathrm{d}r}-\frac{m^2}{r^2}\hat{\varphi}_m+\left(k_{\mathrm{dim}}^2+\frac{\omega^2}{c_{\mathrm{fl}}^2}\right)\hat{\varphi}_m=0, \tag{A.3a}$$

$$\left.\frac{\mathrm{d}\hat{\varphi}_m}{\mathrm{d}r}\right|_{r=R}=-\mathrm{i}\omega C_m. \tag{A.3b}$$

Its solution is

$$\hat{\varphi}_m(r)=-\mathrm{i}\omega C_m J_m\left(r\sqrt{k_{\mathrm{dim}}^2+\frac{\omega^2}{c_{\mathrm{fl}}^2}}\right)\left[\left.\frac{\mathrm{d}J_m\left(r\sqrt{k_{\mathrm{dim}}^2+(\omega^2/c_{\mathrm{fl}}^2)}\right)}{\mathrm{d}r}\right|_{r=R}\right]^{-1}\exp(k_{\mathrm{dim}}x). \tag{A.4}$$

The following non-dimensional parameters are used hereafter:

$$\Omega^2=\frac{\rho(1-v^2)\omega^2R^2}{E},\quad \tilde{\rho}=\frac{\rho}{\rho_{\mathrm{fl}}},\quad \tilde{\gamma}=\frac{c}{c_{\mathrm{fl}}},\quad k=k_{\mathrm{dim}}R,\quad \kappa^2=k^2+\tilde{\gamma}^2\Omega^2.$$

The sound speed in the shell material is introduced as $c^2\equiv E/\rho(1-v^2)$ and the scaled coordinates are $\tilde{r}=(r/R)$, $\tilde{x}=(x/R)$.

Then dispersion equation for a shell filled with a compressible fluid is formulated as

$$\begin{vmatrix} d_{11} & d_{12} & d_{13} \\ d_{21} & d_{22} & d_{23} \\ d_{31} & d_{32} & d_{33} \end{vmatrix} = 0 \tag{A.5}$$

with the following elements:

$$\begin{aligned} d_{11} &= -k^2 + \frac{1-\nu}{2}\, m^2 - \Omega^2, \\ d_{12} &= -\frac{1+\nu}{2}\, km = -d_{21}, \\ d_{13} &= -\nu k = -d_{31}, \\ d_{22} &= -\frac{1-\nu}{2}\, k^2 + m^2 - \Omega^2 - \frac{h^2}{12R^2} 2(1-\nu)k^2 + \frac{h^2}{12R^2} m^2, \\ d_{23} &= m + \frac{h^2}{12R^2}\, m^3 - \frac{h^2}{12R^2}(2-\nu)mk^2 = d_{32}, \\ d_{33} &= 1 + \frac{h^2}{12R^2}\, k^4 - \frac{h^2}{12R^2}\, 2m^2k^2 + \frac{h^2}{12R^2} m^4 - \Omega^2, \\ &\quad - \tilde{\rho}\Omega^2\, \frac{R}{h}\, J_m(\kappa) \left(\frac{\mathrm{d}J_m(\kappa\tilde{r})}{\mathrm{d}\tilde{r}}\bigg|_{\tilde{r}=1} \right)^{-1}. \end{aligned}$$

Appendix B. Green's functions and Somigliana's identities

The boundary integral equations method is based on use of Green's functions and Somigliana identities, which for a fluid-filled pipe are readily available in a closed analytical form

B.1. Green's functions for fluid-filled pipes

Green's function for flexural time-harmonic deformation is a solution to the following differential equation:

$$\left(1 + \frac{h^2}{12R^2}\right) \frac{\partial^4 G_{\mathrm{fl}}(x,\xi)}{\partial x^4} + \Omega^2 \frac{\partial^2 G_{\mathrm{fl}}(x,\xi)}{\partial x^2} - \Omega^2 \left(2 + \frac{\rho_{\mathrm{fl}}}{\rho_0}\, \frac{R}{h}\right) G_{\mathrm{fl}}(x,\xi) = \delta(x-\xi). \tag{B.1}$$

This equation has a unique solution if radiation (Sommerfeld) conditions and decay conditions are imposed at infinity. It has the following form:

$$G_{\mathrm{fl}}(x,\xi) = \frac{1}{4k_1^3} \exp(k_1|x-\xi|) + \frac{1}{4k_2^3} \exp(k_2|x-\xi|), \tag{B.2}$$

k_1 and k_2 are roots of dispersion equation (13), such that $\mathrm{Re}\, k_1 < 0$, $\mathrm{Im}\, k_1 = 0$ and $\mathrm{Re}\, k_2 = 0$, $\mathrm{Im}\, k_2 > 0$.

Green's function for propagation of a torsional wave is a solution of the following differential equation:

$$\left(1 + \frac{h^2}{3R^2}\right) \frac{\partial^2 G_t(x,\xi)}{\partial x^2} + \frac{2\rho\omega^2 R^2(1+\nu)}{E}\, G_t(x,\xi) = -\delta(x-\xi). \tag{B.3}$$

This equation has a unique solution if radiation (Sommerfeld) conditions are imposed at infinity. It has the following form:

$$G_t(x,\xi) = \frac{1}{2k_t} \exp(k_t|x-\xi|), \quad k_t = \mathrm{i}\Omega\sqrt{2(1+\nu)} \left(1 + \frac{h^2}{3R^2}\right)^{-(1/2)}. \tag{B.4}$$

Green's function for propagation of an axial wave is a solution of the following differential equation:

$$\frac{\partial^2 G_{ax}(x,\xi)}{\partial x^2}+\frac{\rho\omega^2 R^2(1-\nu^2)}{E}\,G_{ax}(x,\xi)=-\delta(x-\xi). \tag{B.5}$$

This equation has a unique solution if radiation (Sommerfeld) conditions are imposed at infinity. It has the following form:

$$G_{ax}(x,\xi)=\frac{1}{2k_a}\exp(k_a|x-\xi|),\quad k_a=\mathrm{i}\Omega. \tag{B.6}$$

B.2. Somigliana identities for fluid-filled pipes

Flexural deformation in a horizontal plane, see Fig. 1

$$\begin{aligned} w(\xi)=&-\left(1+\frac{h^2}{12R^2}\right)\left[\frac{\mathrm{d}^3 w(x)}{\mathrm{d}x^3}\,G_{\mathrm{fl}}(x,\xi)-\frac{\mathrm{d}^2 w(x)}{\mathrm{d}x^2}\,\frac{\partial G_{\mathrm{fl}}(x,\xi)}{\partial x}+\frac{\mathrm{d}w(x)}{\mathrm{d}x}\,\frac{\partial^2 G_{\mathrm{fl}}(x,\xi)}{\partial x^2}-\frac{\partial^3 G_{\mathrm{fl}}(x,\xi)}{\partial x^3}\,w(x)\right]\Bigg|_{x=a}^{x=b}\\ &+\int_a^b\frac{(1-\nu^2)Rq_z(x)}{Eh}\,G_{\mathrm{fl}}(x,\xi)\,\mathrm{d}x, \end{aligned} \tag{B.7}$$

$$\begin{aligned} \frac{\mathrm{d}w(\xi)}{\mathrm{d}\xi}=&-\left(1+\frac{h^2}{12R^2}\right)\left[\frac{\mathrm{d}^3 w(x)}{\mathrm{d}x^3}\,\frac{\partial G_{\mathrm{fl}}(x,\xi)}{\partial\xi}-\frac{\mathrm{d}^2 w(x)}{\mathrm{d}x^2}\,\frac{\partial^2 G_{\mathrm{fl}}(x,\xi)}{\partial x\,\partial\xi}+\frac{\mathrm{d}w(x)}{\mathrm{d}x}\,\frac{\partial^3 G_{\mathrm{fl}}(x,\xi)}{\partial x^2\,\partial\xi}\right.\\ &\left.-\frac{\partial^4 G_{\mathrm{fl}}(x,\xi)}{\partial x^3\,\partial\xi}\,w(x)\right]\Bigg|_{x=a}^{x=b}+\int_a^b\frac{(1-\nu^2)Rq_z(x)}{Eh}\,\frac{\partial G_{\mathrm{fl}}(x,\xi)}{\partial\xi}\,\mathrm{d}x. \end{aligned} \tag{B.8}$$

Flexural deformation in a vertical plane, see Fig. 1

$$\begin{aligned} v(\xi)=&-\left(1+\frac{h^2}{12R^2}\right)\left[\frac{\mathrm{d}^3 v(x)}{\mathrm{d}x^3}\,G_{\mathrm{fl}}(x,\xi)-\frac{\mathrm{d}^2 v(x)}{\mathrm{d}x^2}\,\frac{\partial G_{\mathrm{fl}}(x,\xi)}{\partial x}+\frac{\mathrm{d}v(x)}{\mathrm{d}x}\,\frac{\partial^2 G_{\mathrm{fl}}(x,\xi)}{\partial x^2}\right.\\ &\left.-\frac{\partial^3 G_{\mathrm{fl}}(x,\xi)}{\partial x^3}\,v(x)\right]\Bigg|_{x=a}^{x=b}+\int_a^b\frac{(1-\nu^2)Rq_y(x)}{Eh}\,G_{\mathrm{fl}}(x,\xi)\,\mathrm{d}x, \end{aligned} \tag{B.9}$$

$$\begin{aligned} \frac{\mathrm{d}v(\xi)}{\mathrm{d}\xi}=&-\left(1+\frac{h^2}{12R^2}\right)\left[\frac{\mathrm{d}^3 v(x)}{\mathrm{d}x^3}\,\frac{\partial G_{\mathrm{fl}}(x,\xi)}{\partial\xi}-\frac{\mathrm{d}^2 v(x)}{\mathrm{d}x^2}\,\frac{\partial^2 G_{\mathrm{fl}}(x,\xi)}{\partial x\,\partial\xi}+\frac{\mathrm{d}v(x)}{\mathrm{d}x}\,\frac{\partial^3 G_{\mathrm{fl}}(x,\xi)}{\partial x^2\,\partial\xi}\right.\\ &\left.-\frac{\partial^4 G_{\mathrm{fl}}(x,\xi)}{\partial x^3\,\partial\xi}\,v(x)\right]\Bigg|_{x=a}^{x=b}+\int_a^b\frac{(1-\nu^2)Rq_y(x)}{Eh}\,\frac{\partial G_{\mathrm{fl}}(x,\xi)}{\partial\xi}\,\mathrm{d}x. \end{aligned} \tag{B.10}$$

Axial deformation

$$u(\xi)=\left[\frac{\mathrm{d}u(x)}{\mathrm{d}x}\,G_{ax}(x,\xi)-\frac{\partial G_{ax}(x,\xi)}{\partial x}\,u(x)\right]\Bigg|_{x=a}^{x=b}+\int_a^b\frac{(1-\nu^2)Rq_x(x)}{Eh}\,G_{ax}(x,\xi)\,\mathrm{d}x. \tag{B.11}$$

Torsion deformation

$$\phi(\xi)=\left(1+\frac{h^2}{3R^2}\right)\left[\frac{\mathrm{d}\phi(x)}{\mathrm{d}x}\,G_t(x,\xi)-\frac{\partial G_t(x,\xi)}{\partial x}\,\phi(x)\right]\Bigg|_{x=a}^{x=b}+\int_a^b\frac{(1-\nu^2)Rq_t(x)}{Eh}\,G_t(x,\xi)\,\mathrm{d}x. \tag{B.12}$$

Appendix C. Continuity and equilibrium conditions

For convenience, this appendix contains figures illustrating the sign convention adopted in this paper and an explicit formulation of continuity conditions for planar and spatial branching considered in Section 4. (Fig. C)

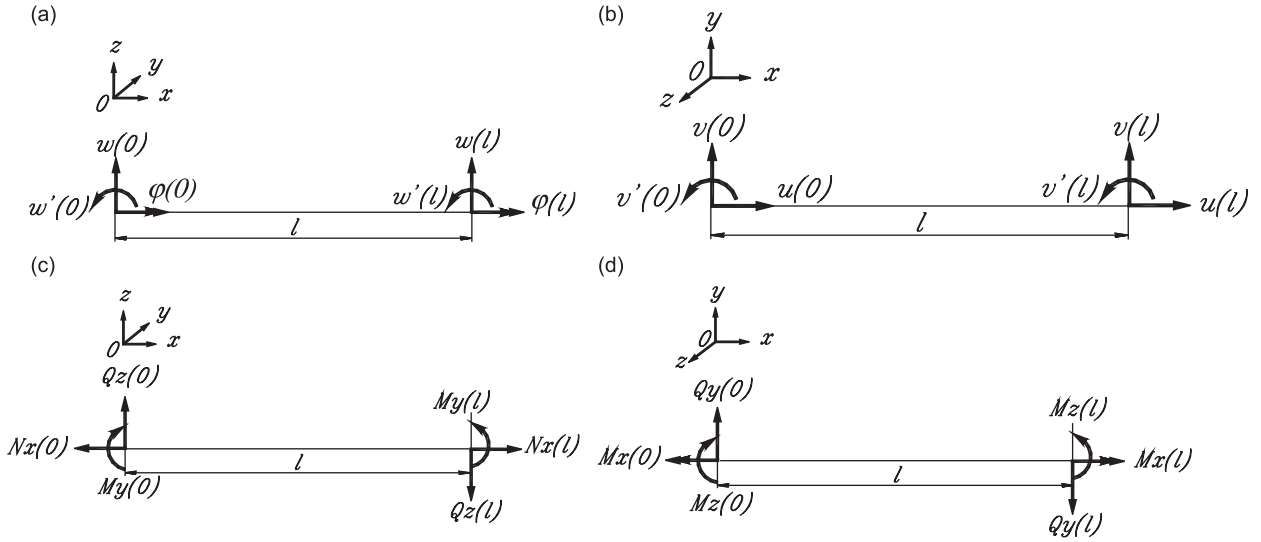

Fig. C. Sign convention for (a) flexural and torsional generalised displacements, (b) flexural and longitudinal generalised displacements, (c) flexural and longitudinal generalised forces and (d) flexural and torsional generalised forces (L_0 is designated as l).

C.1. Planar branching (see Fig. 4)

The continuity conditions are formulated as follows:

$$
\begin{aligned}
&u_1(L_0) = u_2(0)\cos\alpha - v_2(0)\sin\alpha = u_3(0),\\
&\phi_1(L_0) = \phi_2(0)\cos\alpha + w_2'(0)\sin\alpha = \phi_3(0),\\
&v_1(L_0) = u_2(0)\sin\alpha + v_2(0)\cos\alpha = v_3(0),\\
&v_1'(L_0) = v_2'(0) = v_3'(0),\\
&w_1(L_0) = w_2(0) = w_3(0),\\
&w_1'(L_0) = -\phi_2(0)\sin\alpha + w_2'(0)\cos\alpha = w_3'(0).
\end{aligned}
$$

The equilibrium conditions are:

$$
\begin{aligned}
&N_{x1}(L_0) - Q_{y2}(0)\sin\alpha - N_{x2}(0)\cos\alpha - N_{x3}(0) = 0,\\
&Q_{y1}(L_0) + N_{x2}(0)\sin\alpha - Q_{y2}(0)\cos\alpha - Q_{y3}(0) = 0,\\
&Q_{z1}(L_0) - Q_{z2}(0) - Q_{z3}(0) = 0,\\
&M_{x1}(L_0) - M_{y2}(0)\sin\alpha - M_{x2}(0)\cos\alpha - M_{x3}(0) = 0,\\
&M_{y1}(L_0) + M_{x2}(0)\sin\alpha - M_{y2}(0)\cos\alpha - M_{y3}(0) = 0,\\
&M_{z1}(L_0) - M_{z2}(0) - M_{z3}(0) = 0.
\end{aligned}
$$

C.2. Spatial branching (see Fig. 11)

The continuity conditions are formulated as follows:

$$
\begin{aligned}
&u_1(L_0) = -v_2(0) = u_3(0)\cos\beta + w_3(0)\sin\beta,\\
&\phi_1(L_0) = w_2'(0) = \phi_3(0)\cos\beta + v_3'(0)\sin\beta,\\
&w_1(L_0) = w_2(0) = -u_3(0)\sin\alpha + w_3(0),\\
&w_1'(L_0) = -\phi_2(0) = w_3'(0),\\
&w_1(L_0) = w_2(0) = w_3(0),\\
&v_1'(L_0) = v_2'(0) = -\phi_3(0)\sin\beta + v_3'(0)\cos\beta.
\end{aligned}
$$

The equilibrium conditions are:

$$
\begin{aligned}
&N_{x1}(L_0) - N_{x3}(0)\cos\beta + Q_{z3}(0)\cos\beta - Q_{y2}(0) = 0,\\
&Q_{z1}(L_0) - N_{x3}(0)\sin\beta - Q_{z3}(0)\cos\beta - Q_{z2}(0) = 0,\\
&Q_{y1}(L_0) + N_{x2}(0) - Q_{y3}(0) = 0,\\
&M_{x1}(L_0) - M_{x3}(0)\cos\beta - M_{z3}(0)\sin\beta - M_{y2}(0) = 0,\\
&M_{z1}(L_0) + M_{x3}(0)\sin\beta - M_{z3}(0)\cos\beta - M_{z2}(0) = 0,\\
&M_{y1}(L_0) + M_{x2}(0) - M_{y3}(0) = 0.
\end{aligned}
$$

References

[1] S.V. Sorokin, O.A. Ershova, Analysis of the energy transmission in non-uniform cylindrical shells with and without internal heavy fluid loading by boundary equations and by Floquet theory, *Journal of Sound and Vibration* 291 (2006) 81–99.

[2] S.V. Sorokin, N. Olhoff, O.A. Ershova, The energy generation and transmission in compound elastic cylindrical shells with heavy internal fluid loading—from parametric studies to optimization, *Journal of Structural and Multidisciplinary Optimization* 32 (2006) 85–98.

[3] L. Cremer, M. Heckl, *Structure-Borne Sound: Structural Vibrations and Sound Radiation at Audio Frequencies*, Springer, Berlin, 1973.

[4] J.F. Doyle, *Wave Propagation in Structures*, Springer, Berlin, 1997.

[5] M. Paidoussis, *Fluid–Structure Interaction: Slender Structures and Axial Flow*, Vol. 1, Academic Press, New York, 1998.

[6] Y.P. Guo, Flexural wave transmission through angled structural joints, *Journal of Acoustical Society of America* 97 (1995) 289–297.

[7] S. Finneveden, Spectral finite element analysis of the vibration of straight fluid-filled pipes with flanges, *Journal of Sound and Vibration* 199 (1997) 125–154.

[8] M. Oiusse, J.L. Guyader, Vibration sensitive behaviour of a connecting angle. Case of coupled beams and plates, *Journal of Sound and Vibration* 267 (2003) 809–850.

[9] S.V. Sorokin, O.A. Ershova, Plane wave propagation and frequency band gaps in periodic plates and cylindrical shells with and without heavy fluid loading, *Journal of Sound and Vibration* 278 (2004) 501–526.

[10] S.V. Sorokin, A.V. Terentiev, Flow-induced vibrations of an elastic cylindrical shell conveying a compressible fluid, *Journal of Sound and Vibration* 296 (2006) 777–796.

[11] C.R. Fuller, F.J. Fahy, Characteristics of wave propagation and energy distributions in cylindrical shells filled with fluid, *Journal of Sound and Vibration* 81 (4) (1982) 501–518.

[12] C.R. Fuller, The input mobility of an infinite circular cylindrical shell filled with fluid, *Journal of Sound and Vibration* 87 (3) (1983) 409–427.

[13] G. Pavic, Vibroacoustical energy flow through straight pipes, *Journal of Sound and Vibration* 154 (3) (1992) 411–429.

[14] S. Finneveden, Simplified equations of motion for the radial-axial vibrations of fluid filled pipes, *Journal of Sound and Vibration* 208 (1997) 685–703.

[15] A.L. Gol'denvejzer, V.B. Lidskij, P.E. Tovstik, *Free Vibrations of Thin Elastic Shells*, Nauka, Moscow, 1979 (in Russian).

[16] M.L. Munjal, *Acoustics of Ducts and Mufflers*, Wiley-Interscience, New York, 1987.

[17] M. Aabom, Derivation of the four-pole parameters includind higher order mode effects for expansion chamber mufflers with extended inlet and outlet, *Journal of Sound and Vibration* 137 (1990) 403–418.

[18] S.V. Sorokin, O.V. Krylova, The boundary equation method for analysis of stationary vibrations and energy flows in spatial finite and semi-infinite structures composed of tubular elements, *Proceedings of the 30th Summer School—Conference "Advanced Problems in Mechanics"*, St. Petersburg, Russia, 2004, pp. 246–249.

[19] J.D. Kaplunov, S.V. Sorokin, A simple example of a trapped mode in an unbounded wave guide, *Journal of Acoustical Society of America* 97 (6) (1995) 3898–3899.